*Original article*

# Capillary pressure–saturation curves of thin hydrophilic fibrous layers: effects of overburden pressure, number of layers, and multiple imbibition–drainage cycles

**Amir Hossein Tavangarrad**[1] ⓘ**, S. Majid Hassanizadeh**[1]**,
Rodrigo Rosati**[2]**, Luigi Digirolamo**[2] **and
Martinus Th van Genuchten**[1,3]

## Abstract
Unsaturated fluid flow in thin porous media depends on hydraulic properties, such as the capillary pressure, $P_c$, as a function of saturation, $S$. We measured this relationship for two different types of compressible thin hydrophilic fibrous layers under varying conditions. Among other factors, we changed the number of layers and the overburden pressure (i.e. the confined solid pressure applied on top of the sample) imposed on one layer or a stack of layers. Applying an overburden pressure drastically affected the $P_c(S)$ curves. However, increasing the number of fibrous layers had little impact on the capillary pressure–saturation curves. We also investigated the effect of multiple imbibition–drainage cycles on the $P_c(S)$ data. Measured data points were used to find general expressions for the $P_c(S)$ relationships of compressible thin porous media. Existing quasi-empirical correlations used in vadose zone hydrology, notably expressions by van Genuchten (Van Genuchten MTh. A closed-form equation for predicting the hydraulic conductivity of unsaturated soils. *Soil Sci Soc Am J* 1980; 44: 892-898) and Durner (Durner W. Hydraulic conductivity estimation for soils with heterogeneous pore structure. *Water Resour Res* 1994; 32: 211–223) for single- and dual-porosity media, respectively, were employed to fit the measured data points.

Thin nonwoven fabrics have many applications, such as for use in hygiene products, clothes, filters, and fuel cells.[1–6] The hydraulic characteristics of a thin fibrous layer have great impact on the performance of fibrous products. Knowledge of the hydraulic properties of thin fabrics is hence essential for optimizing the performance of these products. Unfortunately, there are several challenges when measuring the unsaturated hydraulic properties of such thin layers. A layer is considered physically thin when the number of pores along its thickness is less than approximately 15 [see Qin and Hassanizadeh,[7,8] Ceballos et al.,[9] and Tavangarrad et al.[10]], with the thickness of a thin porous layer obviously being much smaller than its planar extent.

A number of studies focusing on measurement of the capillary pressure–saturation relationships of thin nonwoven fabrics are reported in the literature. Several concern the $P_c(S)$ curves of water–air systems in the gas diffusion layer (GDL) of polymer electrolyte fuel cells (PEFCs) [see Sole,[11] Gostick et al.,[12,13]

[1]Department of Earth Sciences, Environmental Hydrogeology Group, Utrecht University, The Netherlands
[2]Procter & Gamble Service GmbH, Germany
[3]Center for Environmental Studies, CEA, São Paulo State University, Brazil

**Corresponding author:**
Amir Hossein Tavangarrad, Department of Earth Sciences, Environmental Hydrogeology Group, Utrecht University, Princetonplein 9, 3584CC Utrecht, The Netherlands.
Email: A.H.Tavangarrad@uu.nl

Nguyen et al.,[14,15] Kumbur et al.,[16,17] Fairweather et al.,[18] Jena and Gupta[19]]. A comprehensive review of available techniques employed for GDLs is reported in a study by Sole.[11] Some measurements have been carried out also to determine the $P_c(S)$ relationships of thin hydrophilic fabrics used in medical and hygienic absorbent products.[10,20,21]

Several modeling studies also exist to estimate the capillary pressure–saturation curves of thin fibrous layers. For example, in a recent study, general expressions for the $P_c(S)$ relationship of thin fabrics were developed for a family of fibrous media using a pore morphology methodology.[22] That work, however, was based on virtual nonwoven fibrous materials. Pore morphology modeling has been used also to determine the $P_c(S)$ relationship of uncoated thin paper.[23]

A few studies can be found in the literature on changes in the $P_c(S)$ curves of thin fabrics due to the effect of an overburden pressure. In an experimental study by Kumbur et al.,[17] the effect of compression on the drainage capillary pressure–saturation curve of thin fibrous layers with mixed wettability was investigated. Another study concerned the image analysis of compression-induced morphological changes of nonwoven fibrous materials.[24] Furthermore, Jena and Gupta[25] investigated the influence of overburden effects on the pore structure of battery separators made of nonwoven fibrous layers. These various studies, however, focused on changes in the pore-size distribution rather than capillary-pressure–saturation curves.

To the best of our knowledge, the effects of overburden pressure, the occurrence of multiple imbibition–drainage cycles, and the number of layers on the imbibition–drainage $P_c(S)$ relationships of thin hydrophilic nonwoven fabrics have not been studied experimentally thus far. These different effects are encountered in many practical applications. Examples are hygienic products such as diapers, in which the weight of a baby imposes compression on the stack of thin fibrous layers. The compression effect is also a key factor in the optimization of fuel cell stack assemblies. Multiple imbibition–drainage cycles occur in many products, such as diapers, adult incontinence products, and absorption pads. The number of imbibition–drainage cycles is then different depending upon the volume of liquid in each gush of fluid, and the maximum available pore volume for fluid storage.

For our study we used an autoporosimetry technique developed by Miller and Tomkin[26] to characterize thin hydrophilic nonwoven fabrics. Our objective was to evaluate the effects of three main factors on the capillary pressure–saturation relationship of thin hydrophilic nonwoven fabrics: the number of layers, overburden pressure, and number of imbibition–drainage cycles. Measurements were performed on

thin layers made of two different synthetic polymers. A comprehensive study was carried out to determine the $P_c(S)$ curves of compressed and uncompressed thin fabrics. The individual data points were fitted with the relationships proposed by van Genuchten (VG)[27] and Durner[28] for single- and dual-porosity media, respectively. We also investigated the effects of overburden pressure on porosity and permeability changes of the thin layers.

The remainder of this paper is organized as follows. In the second section, the experimental setup and procedure are briefly described. The fitting function are also introduced in this section. In the third section, influences of the overburden pressure, the number of layers, multiple imbibition-drainage cycles, and the layer material on the capillary pressure-saturation measurements are discussed. Finally, scaling $P_c(S)$ curves using the Leverett J-function are described in the fourth section, followed by conclusions in the fifth section.

## Methods and material

### Materials

Two different nonwoven fabrics were used in this study: polyolefin fabric and polyethylene terephthalate (PET) fabric. The layers were made of polyolefin fabric thermally bonded in some regions during the production process. They were also treated with a surfactant to make them hydrophilic. Each layer was about 260 μm thick with a porosity of approximately 90%. The PET fabric was made of hollow fibers. The PET layer was about 1500 μm thick with a porosity of close to 97%. The porosity value was calculated from the maximum uptake of the layer based on the following equation

$$\varphi = \frac{m_{\max}^l}{m_{\max}^l + \frac{\rho^l}{\rho^f} m^s} \qquad (1)$$

where $m_{\max}^l$ is the maximum mass of the liquid phase, $m^s$ is the solid mass of the fibrous layer, $\rho^l$ is the liquid density, and $\rho^f$ the fiber density. The fiber content was distributed symmetrically across both layer materials. The fiber content variation of the polyolefin-based material versus depth was found to have the form of a bell-shaped function. Other properties of the materials, including fiber radius and density values, are given in Table 1.

A saline solution, made of 0.9% NaCl (by weight) and distilled water, was chosen as the working liquid. The solution had a surface tension of 72.5 mN/m, a density of 1.005 g/cm³, and a viscosity of 1.019 mPa.s. Both fibrous materials exhibited negligible swelling in such a solution.[1]

## Experimental setup

The setup used in this study to measure capillary pressure and saturation is referred to as a PVD-Autoporosimeter (Pore Volume Distribution Autoporosimeter), as developed by Miller and Tyomkin.[26] A schematic view and a picture of the setup is shown in Figure 1. The PVD-Autoporosimeter consisted of two parts: a chamber containing the fabric sample and a solution reservoir. The sample chamber consisted of a glass frit, a membrane, a tube to connect the chamber to the reservoir, an electronic balance, and an automatic system to control the pressure and temperature of air in the headspace. The membrane covered the glass frit, while the circular sample with a diameter of 50 mm was placed on the membrane. A weight could be placed on the sample to provide compression loading. The solution reservoir was placed on a high-precision balance. The reservoir was covered by a lid to minimize evaporation, while still being connected to atmospheric air. The water level in the reservoir was set equal to the same elevation as the top of the membrane. Changes in the water level due to drainage or imbibition of the sample could be considered negligible, since the lateral surface area was relatively large.

**Table 1.** Properties of the two fibrous layers used in this study

| Properties | Unit | Polyolefin | PET |
|---|---|---|---|
| Fiber radius | [μm] | 10 | 16 |
| Fiber density | [g/cm$^3$] | 0.92 | 1.35 |
| Porosity (compressed) | [−] | 0.84 | 0.93 |
| Porosity (uncompressed) | [−] | 0.90 | 0.97 |
| Permeability (compressed) | [m$^2$] | $8.29 \times 10^{-11}$ | $1.46 \times 10^{-9}$ |
| Permeability (uncompressed) | [m$^2$] | $2.05 \times 10^{-10}$ | $5.10 \times 10^{-9}$ |
| Thickness (compressed) | [μm] | 200 | 900 |
| Thickness (uncompressed) | [μm] | 260 | 1500 |

PET: polyethylene terephthalate.

## Experimental procedure

The PVD-Autoporosimeter was used to obtain capillary pressure–saturation curves based on quasi-static multi-step inflow–outflow measurements. Capillary pressures were varied by increasing or decreasing the air pressure during drainage and imbibition, respectively. Water pressures in the sample were assumed to remain equal to atmospheric pressure at equilibrium since they were at the same level as the level of the solution reservoir. Air pressure steps were specified in the PVD-Autoporosimeter software and fed into an automatic controller, which could change the air pressure in the chamber. Fluid saturation values of the sample were measured gravimetrically using the balance. At each step, the air pressure was kept constant until equilibrium was reached and capillary flow had ceased. A few hours were needed to perform a full imbibition–drainage cycle. We note that a slight loss of weight of the solution reservoir was still recorded due to evaporation, which could not be neglected completely despite the reservoir being covered by a lid. The evaporation rate was determined from the mass loss of the reservoir as measured for an extended period of time. During measurement of the $P_c(S)$ curves, we assumed that equilibrium was reached when the reservoir mass loss rate became less than some small threshold value. The experimental results were corrected by taking the measured evaporation rate into an account. More information about the equilibrium threshold is given in Appendix B (Supplemental material available online).

The glass frit and membrane were kept fully saturated at all times. Sometimes during imbibition a few droplets of water formed on the membrane surface, but disappeared during drainage. Also, a very small volume of water ($\cong 200\,\mu$l) could accumulate around the edge of the membrane at the bottom due to capillary rise against the wall of the chamber in the form of a corner triangle. Such effects are negligible for $P_c(S)$ measurements of large porous samples (such as soil
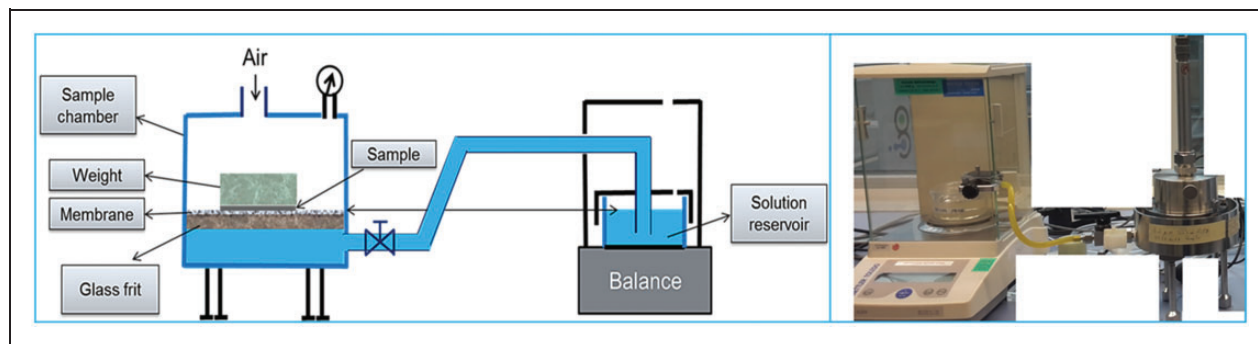


**Figure 1.** Schematic view and picture of the Pore Volume Distribution Autoporosimeter.

samples). However, because of the very small pore volumes involved, they cannot be neglected in the case of thin layers. In order to reduce this effect, we modified the setup. This reduced the capillary rise volume to about 40 µl. Therefore, in order to reduce uncertainty and measurement errors, the corresponding volume of water was quantified in blank measurements (without any sample) at various air pressures. The mass loss or gain of the reservoir during $P_c(S)$ measurements of the layers was corrected using this blank volume. More details about this correction are provided in Appendix A (Supplemental material available online).

## Fitting of data points

Equations commonly used for describing observed capillary pressure–saturation data are those proposed by VG,[27] Brooks and Corey (BC),[29] and Durner,[28] among others. The VG formula is given by

$$S_e(h) = \frac{1}{(1 + |\alpha h|^n)^m} \qquad (2)$$

where $h$ is the capillary pressure head, $\alpha$ and $n$ are fitting parameters, $m = 1 - 1/n$, and $S_e$ is effective saturation given by $S_e = (S - S_{ir})/(1 - S_{ir})$, in which $S$ is the degree of fluid saturation and $S_{ir}$ is irreducible saturation. Because of the very large porosity of our samples, no residual air saturation needed to be considered. In physical terms, $\alpha$ corresponds approximately to the inverse of the non-wetting phase entry pressure, while the value of $n$ reflects the pore-size distribution. Another formula is the BC equation[29]

$$S_e(h) = \left(\frac{h}{h_e}\right)^{-\lambda}; \quad \text{for} \quad h > h_e \qquad (3)$$

where $h_e$ is the air entry pressure head, while $\lambda$ is often referred to as the pore-size distribution index. For more complex cases, the Durner bimodal function, which is constructed by linear superposition of VG sub-curves, may be needed

$$S_e(h) = \frac{w_f}{(1 + |\alpha_f h|^{n_f})^{m_f}} + \frac{w_m}{(1 + |\alpha_m h|^{n_m})^{m_m}} \qquad (4)$$

where $\alpha_f, n_f, \alpha_m, n_m$ are fitting parameters, $w_f$ and $w_m$ are weights of the overlapping regions (subject to $w_f + w_m = 1$), $m_f = 1 - 1/n_f$, and $m_m = 1 - 1/n_m$.

The above equations may be used for woven or nonwoven fabrics under both compressed and uncompressed conditions. The VG and BC equations are appropriate for unimodal $P_c(S)$ curves, while Durner's equation (and extensions thereof) can be applied to bimodal (and multi-modal) curves. For instance,

Gostick et al.[13] only used unimodal VG- and BC-based $P_c(S)$ curves for their thin fibrous GDLs. Bimodal models such as Durner's equation should provide better descriptions of some of their $P_c(S)$ data sets.

## Results

### Influence of overburden pressure

To study the effect of overburden pressure on the capillary pressure–saturation curves, the $P_c(S)$ curves of a single polyolefin layer were measured with and without placing a metal weight on top of the sample. We also studied the effect of compression on the porosity of the fabric. When putting a 0.3 psi metal weight on top of the polyolefin fabric, the porosity was reduced from 0.9 to 0.84. The measured imbibition and drainage curves with and without compression were both found to be significantly different also, as shown in Figure 2. The error bars in this figure are based on duplicate measurements. Higher capillarity was observed with the overburden pressure as compared to the uncompressed layer. This is because the mean pore size becomes smaller when the fabric carries a metal weight. Jaganathan et al.[24] observed similar effects on the mean pore size of a hydroentangled nonwoven fabric when exposed to an overburden pressure, based on Digital Visual Interface (DVI) image analyses. We also observed that during drainage both curves showed a bimodal character, which was much more pronounced for the compressed sample. This can be attributed to having pores near the surface with a different size distribution than the rest of the layer. This effect is far less important in the case of compressed layers.

The parameters of the fitted imbibition and drainage curves shown in Figure 2 are listed in Table 2. The VG equation was found to fit the imbibition data points satisfactorily. However, Durner's formula could fit the drainage data of both the compressed and uncompressed layers much better. The higher value of $\alpha$ for the imbibition curve of the uncompressed layer, compared to the compressed layer, showed that the air entry pressure was lower for the uncompressed fabric. Similarly, corresponding $\alpha_f$ and $\alpha_m$ values of Durner's equation fitted to the drainage data of the uncompressed layer were larger than those of the compressed layer. A larger value of $n_m$ in Durner's formula was obtained for the compressed layer, which indicates a sharper transition of saturation at larger capillary pressures compared to the uncompressed layer within the same range.

The bimodal porosity is indeed expected to affect the shape of both drainage and imbibition curves. This effect, however, is not pronounced in the case of imbibition because it occurs in a much narrower saturation range. This is also the main reason why we could not get many

data points during the imbibition process. We could have tried to fit the imbibition data using the bimodal formula; however, since only a few data points were available, one of the weighting coefficients became very close to zero. This suggests that two fitting parameters were sufficient for fitting the imbibition data points.

## Influence of the number of layers

One fibrous layer, or a stack of two or five layers, of polyolefin was placed on top of the membrane in the sample chamber and exposed to an overburden pressure of 0.3 psi (about 2 kPa). Capillary pressure–saturation data for the compressed stack were collected for both imbibition and drainage. The influence of increasing the number of polyolefin layers on the $P_c(S)$ curves is shown in Figure 3. The error bars in this figure are based on the standard deviation of two replicates of the same experiment. Results indicate no significant difference between the drainage data for different stacks of layers. VG fitting parameters of the drainage curves, shown in Table 3, confirm the similarity of the various

curves. Differences are within the effect of variability in the sample material itself. Although small differences exist in the imbibition data, this had only a marginal effect on the fitted curves. The fitted parameter values of the imbibition curves are given in Table 3.

A similar comparison was made between the $P_c(S)$ curves of a single polyolefin layer and stacks of multiple layers without overburden pressure. The results are shown in Figure 4. Slightly higher saturation values were obtained for a single layer as compared to multiple layers for saturations from zero up to about 50% during drainage. Beyond this saturation, the trend reversed and the stacks of multiple layers had higher saturation values compared to a single layer. Nevertheless, differences between the measured curves are relatively minor. We conclude that the number of layers has little impact on measured capillary pressure–saturation data points, especially for uncompressed layers.

## Influence of multiple imbibition–drainage cycles

We next investigated the effect of multiple imbibition–drainage cycles on the hydraulic properties of a single
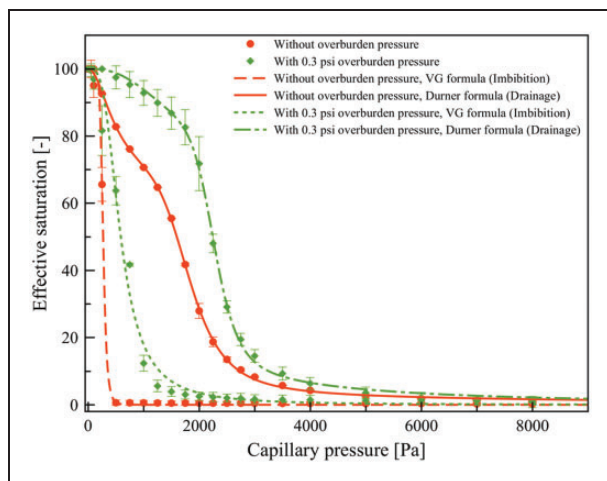


**Figure 2.** Measured capillary pressure–saturation data for a single polyolefin layer with and without overburden pressure. Lines show curves fitted to the data using van Genuchten (VG) and Durner formulas.
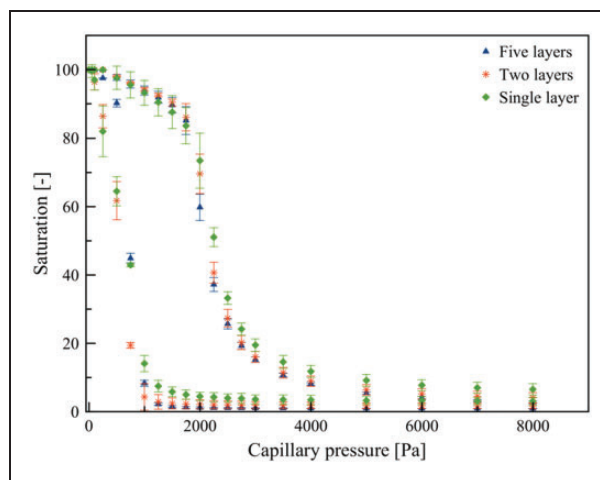


**Figure 3.** Capillary pressure–saturation data for different sets of polyolefin layers under 0.3 psi overburden pressure.
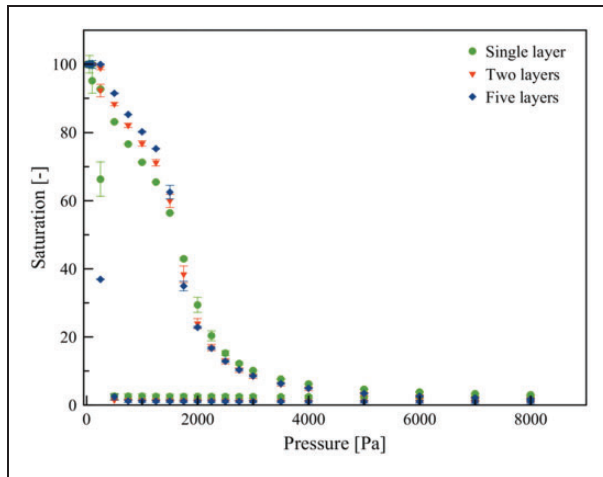
**Table 2.** Fitting parameters of imbibition and drainage curves of a compressed and an uncompressed single polyolefin layer

|  | Imbibition VG formula $\alpha$ [1/Pa] | Imbibition VG formula $n$ [−] | Irreducible saturation $S_{ir}$ [−] | Drainage Durner formula $w_f, w_m$ [−] | Drainage Durner formula $\alpha_f$ [1/Pa], $\alpha_m$ [1/Pa] | Drainage Durner formula $n_f, n_m$ [−] |
|---|---|---|---|---|---|---|
| Uncompressed polyolefin | 0.00378 | 8.53 | 0.02 | 0.42, 0.58 | 0.00260, 0.00056 | 2.07, 6.64 |
| Compressed polyolefin | 0.00197 | 3.44 | 0.06 | 0.35, 0.65 | 0.00069, 0.00044 | 2.63, 11.80 |

VG: van Genuchten.

**Table 3.** Van Genuchten fitting parameters of the imbibition and drainage curves of compressed samples containing different numbers of polyolefin layers

| Sample | Imbibition $\alpha$ [1/Pa] | Imbibition $n$ [−] | Drainage $\alpha$ [1/Pa] | Drainage $n$ [−] |
|---|---|---|---|---|
| Single layer | 0.00197 | 3.44 | 0.000469 | 6.29 |
| Stack of two layers | 0.00197 | 5.04 | 0.000475 | 7.16 |
| Stack of five layers | 0.00143 | 7.24 | 0.000488 | 6.62 |



**Figure 5.** Effect of multiple imbibition–drainage cycles on capillary pressure–saturation measurements of a single polyolefin layer subject to overburden pressure.
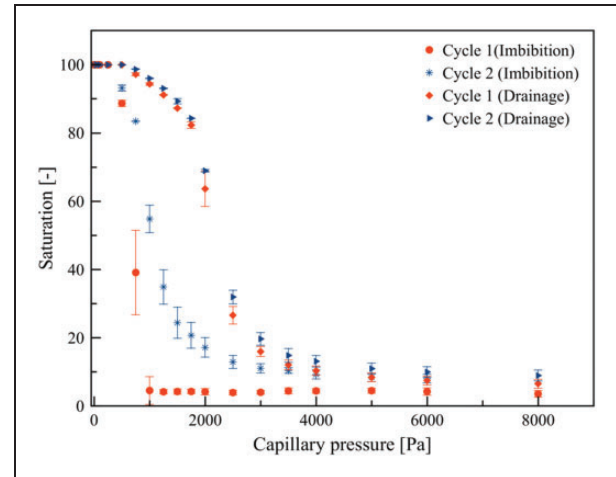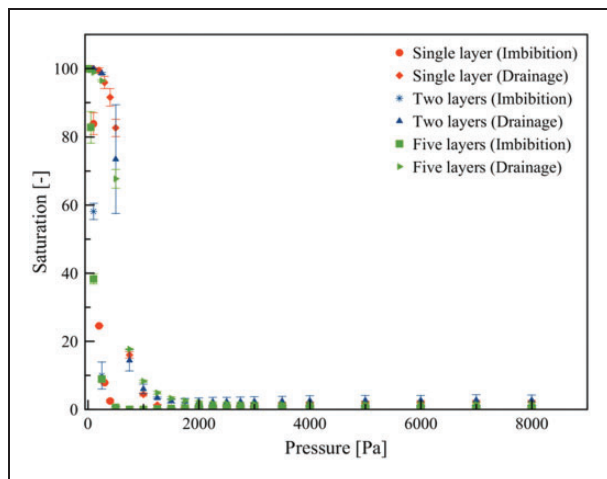


**Figure 4.** Capillary pressure–saturation data points for different numbers of polyolefin layers without applying overburden pressure.

polyolefin layer, starting with a dry sample subject to an overburden pressure of 0.3 psi. Figure 5 shows results for two consecutive imbibition–drainage cycles. No significant difference is apparent for the drainage data, except for a clear shift in the imbibition data points toward higher saturation and capillary pressures.

The main reason for this effect is the fact that dry polyolefin fibers have a low surface energy and are receptive to being wetted by water. At the start of the second imbibition cycle, the fibers already contained some fluid (because of an irreducible saturation of around 6%). Surface energies as a result increased, leading to higher capillary pressures at given saturation levels.

## Effect of layer material

The experiments thus far were carried out using polyolefin fabric. A similar series of experiments was performed on layers made of PET. The PET layers are thicker than those made of polyolefin, but are much coarser by containing at most 10 pores along their

thickness (Table 1). Fiber diameters and mean pore sizes of the PET layers, as well as their porosity, are larger than those of the polyolefin layer.
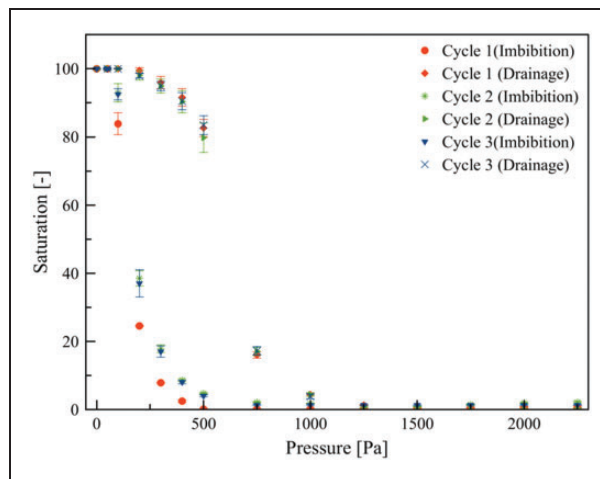
Measured capillary pressure–saturation data for various sets of PET layers are presented in Figure 6. As expected, a lower capillarity for the PET layer was observed during both imbibition and drainage (compare Figures 2 and 6). Values of the VG parameters, obtained by fitting Equation (1) to the data points, are listed in Table 4. Clearly, values of $\alpha$ for the imbibition and drainage curves of the compressed PET layers were much larger than those of the polyolefin layer, as is shown also by the entries in Tables 2 and 3. Similarly, the measured permeability and porosity of PET fabric are much higher.

Results of the capillary pressure–saturation measurements of the stacks with different numbers of PET layers are depicted in Figure 6. The variability in the measurements can be attributed mainly to inherent differences in the fabrication of the fabric. The relatively small difference in the data for different numbers of layers shows that the effect of interlayer space is negligible. This is similar to the results we obtained for the polyolefin stacks, as shown in Figure 3.

Next, the effect of multiple imbibition–drainage cycles was studied on a single PET layer under compressed conditions. The results are shown in Figure 7. The data again did not show any differences between the second and third cycles for both imbibition and drainage. However, similarly as for the polyolefin experiments, the imbibition curves of the second and third cycles exhibited higher capillary pressures compared to the first cycle. Finally, we studied the effect of overburden pressure on the $P_c(S)$ curves of a single PET layer. Figure 8 shows the capillary

**Figure 6.** Capillary pressure–saturation of different numbers of polyethylene terephthalate layers under 0.3 psi overburden pressure.



**Figure 7.** Effect of multiple imbibition/drainage cycles on capillary pressure–saturation measurements of a single polyethylene terephthalate layer.

**Table 4.** Hydraulic parameters of the imbibition and drainage curves of a single compressed polyethylene terephthalate layer used in this study

| Imbibition VG formula $\alpha$ [1/Pa] | Imbibition VG formula $n$ [−] | Irreducible saturation $S_{ir}$ [−] | Drainage VG formula $\alpha$ [1/Pa] | Drainage VG formula $n$ [−] |
|---|---|---|---|---|
| 0.0073 | 4.32 | 0.01 | 0.001698 | 7.71 |

VG: van Genuchten.

pressure–saturation drainage curves with and without the overburden pressure (again 0.3 psi). Corresponding fitting parameters of the $P_c(S)$ drainage curves using the unimodal VG and bimodal Durner models are given in Tables 4 and 5, respectively. The PET results are very much in line with those of the polyolefin fabric, as shown in Figure 3. Higher capillary pressures were obtained with the overburden pressure, since the fabric then deforms and the pores become smaller.

## Scaling of $P_c(S)$ curves using the Leverett $J$-function

The purpose of employing the Leverett $J$-function[30] is to use measured $P_c(S)$ curves of a given nonwoven fibrous material in order to construct $P_c(S)$ curves for similar materials and/or for different conditions. The $P_c(S)$ equation as proposed by Leverett[30] is of the form

$$P_c(S) = \gamma \cos(\theta)\left(\frac{\varphi}{K}\right)^{\frac{1}{2}} J(S) \qquad (5)$$
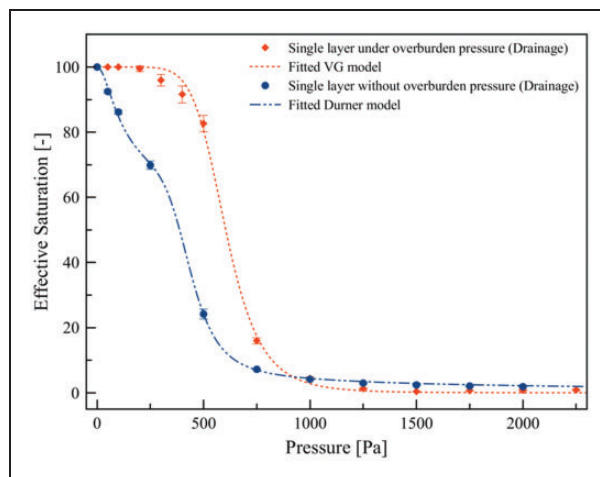


**Figure 8.** Observed (symbols) and fitted (lines) drainage capillary pressure–saturation curves of a single polyethylene terephthalate layer with and without overburden pressure. VG: van Genuchten.

in which $\theta$ is the static contact angle of a fluid–solid system, $\varphi$ is porosity, and $\gamma$ is the interfacial tension between the wetting and non-wetting fluids. The function $J(S)$ presumably is the same for similar media. Udell[31] did propose an equation for $P_c(S)$ for highly hydrophilic geological porous media, which was used later also for thin fibrous layers[32]

$$J(S) = \begin{cases} 1.417(1 - S) - 2.12(1 - S)^2 \\ \qquad + 1.263(1 - S)^3 & \text{for} \quad \theta \leq 90 \\ 1.417S - 2.12S^2 + 1.263S^3 & \text{for} \quad \theta > 90 \end{cases}$$

$$(6)$$

**Table 5.** Fitting parameters of the drainage curve of the uncompressed single polyethylene terephthalate layer used in this study

| Durner formula $w_f, w_m$ [−] | Durner formula $\alpha_f$ [1/Pa], $\alpha_m$ [1/Pa] | Durner formula $n_f, n_m$ [−] | Irreducible saturation $S_{ir}$ [−] |
|---|---|---|---|
| 0.43, 0.57 | 0.012, 0.0023 | 1.94, 7.38 | 0.02 |
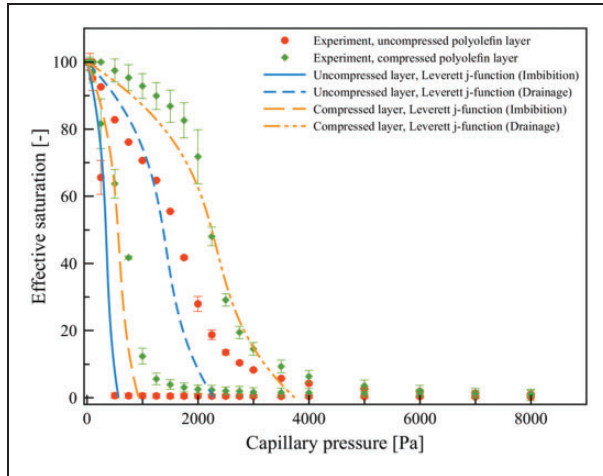


**Figure 9.** Observed and fitted imbibition–drainage curves of a compressed polyolefin layer using Leveret's *J*-function. The fitted curve was used to obtain the $P_c(S)$ curve for an uncompressed layer based on Equation (5).

The generic Leveret approach given by the above equations was used to fit capillary pressure–saturation curves of a compressed polyolefin layer. Assuming the interfacial tension between air and liquid remains constant during the measurements, the only unknown parameter is the static contact angle. The best fit of the drainage data was obtained with a contact angle of 25 degrees, while the imbibition data points were matched using a contact angle of 77 degrees. We thus used Equation (5) to predict the $P_c(S)$ data of an uncompressed nonwoven fibrous material from a similar type of fabric based on equality of the *J*-function for the two fabrics as follows[33]

$$P_{c2}(S) = P_{c1}(S)\frac{\gamma_2}{\gamma_1}\left(\frac{K_1}{K_2}\right)^{\frac{1}{2}}\left(\frac{\varphi_2}{\varphi_1}\right)^{\frac{1}{2}} \quad (7)$$

where the subscripts 1 and 2 denote uncompressed and compressed layers, respectively. The contact angle was assumed to be same for both layers. It should be noted that a change in the contact angle is not the only reason for hysteresis in the capillary pressure–saturation curve. Differences occur also since small pores control drainage events while the larger pore regions control imbibition,[33] often referred to as the ink bottle effect.

As explained in previous studies [e.g. Nguyen et al.[14] and Kumbur et al.[16]], the equations above are insufficient for describing capillary flow phenomena. One should consider such additional variables as pore-size distribution and stress–strain relationships to better scale the $P_c(S)$ curves under different compression loads. However, as illustrated in Figure 9, similar trends in Leveret's -J function, and hence the $P_c(S)$ curves, were obtained due to the overburden pressure effect. The predicted curves could not reproduce the bimodal behavior of the uncompressed layer under the drainage condition. However, as shown by Figure 9, changes in the $P_c(S)$ curves due to hysteresis and the overburden pressure were well reproduced by the Leverett scaling approach.

## Conclusions

In this research we investigated the effect of several factors on the capillary pressure–saturation curves of two different thin nonwoven fibrous materials. Results for both materials demonstrated the important effect of overburden pressure on the $P_c(S)$ curves. However, increasing the number of layers did not seem to affect the curves drastically. In addition, the influence of multiple imbibition–drainage cycles showed that wetting of a sample in the first cycle would increase the capillarity in the next cycles. We used both the unimodal VG and bimodal Durner models to fit the experimental data. The Durner model is recommended when the capillary pressure–saturation data show clear bimodal behavior. One major question that remained unanswered is how the capillary-pressure–saturation function of nonwoven fabric (like that of many medical absorbent products) may change during dynamic flow conditions, as has been noted for other porous media[34] (see Appendix C (Supplemental material available online)). Work on the dynamic capillary pressure–saturation curves is still in progress.

### Declaration of conflicting interests

### Funding

## Supplemental material

Supplemental material is available online for this article.

## ORCID iD

Amir Hossein Tavangarrad (iD) http://orcid.org/0000-0002-3831-1555

## References

1. Albrecht W, Fuchs H and Kittelmann W. *Nonwoven fabrics: raw materials, manufacture, applications, characteristics, testing processes*. Weinheim: Wiley-VCH, 2003.

2. Prat M and Agaësse T. Thin porous media. In: Vafai K (ed.) *Handbook of porous media*, 3rd ed. London: Taylor & Francis, 2015.

3. Liu Z, He X, Han J, et al. Liquid wicking behavior in paper-like materials: mathematical models and their emerging biomedical applications. *Microfluid Nanofluid* 2018; 22: 132.

4. Liu Z, Hu J, Zhao Y, et al. Experimental and numerical studies on liquid wicking into filter papers for paper-based diagnostics. *Appl Therm Eng* 2015; 88: 280–287.

5. Tavangarrad AH. *Experimental and computational study of unsaturated flow in a stack of thin layers, application to non-woven hygiene products*. PhD Thesis, Utrecht University, 2019.

6. Liang S, Pan N, Cui Y, et al. Steam impinging and heat and water spreading in fabrics. *Text Res J* 2018; 89: 1455–1471.

7. Qin CZ and Hassanizadeh SM. Multiphase flow through multilayers of thin porous media: general balance equations and constitutive relationships for a solid-gas-liquid three-phase system. *Int J Heat Mass Transf* 2014; 70: 693–708.

8. Qin CZ and Hassanizadeh SM. A new approach to modelling water flooding in a polymer electrolyte fuel cell. *Int J Hydrogen Energ* 2015; 40: 3348–3358.

9. Ceballos L, Prat M and Duru P. Slow invasion of a non-wetting fluid from multiple inlet sources in a thin porous layer. *Phys Rev E* 2011; 84: 056311.

10. Tavangarrad AH, Mohebbi B, Hassanizadeh SM, et al. Continuum-scale modeling of liquid redistribution in a stack of thin hydrophilic fibrous layers. *Transp Porous Media* 2018; 122: 203–219.

11. Sole JD. *Investigation of water transport parameters and processes in the gas diffusion layer of PEM fuel cells*. PhD Dissertation, Virginia Polytechnic Institute and State University, 2008.

12. Gostick JT, Ioannidis MA, Fowler MW, et al. Direct measurement of the capillary pressure characteristics of water-air-gas diffusion layer systems for PEM fuel cells. *Electrochem Commun* 2008; 10: 1520–1523.

13. Gostick JT, Fowler MW, Ioannidis MA, et al. Capillary pressure and hydrophilic porosity in gas diffusion layers for polymer electrolyte fuel cells. *J Power Source* 2006; 156: 375–387.

14. Nguyen TV, Lin G, Ohn H, et al. Measurement of capillary pressure property of gas diffusion media used in proton exchange membrane fuel cells. *Electrochem Solid State Lett* 2008; 11: B127–B131.

15. Nguyen TV, Guangyu L, Heebong O, et al. Measurements of two-phase flow properties of the porous media used in PEM fuel cells. *ECS Trans* 2006; 3: 415–423.

16. Kumbur EC, Sharp KV and Mench MM. Validated Leverett approach for multiphase flow in PEFC diffusion media, I. Hydrophobicity effect. *J Electrochem Soc* 2007; 154: B1295–B1304.

17. Kumbur EC, Sharp KV and Mench MM. Validated Leverett approach for multiphase flow in PEFC diffusion media, II. Compression effect. *J Electrochem Soc* 2007; 154: B1305–B1314.

18. Fairweather JD, Cheung P, St-Pierre J, et al. A microfluidic approach for measuring capillary pressure in PEMFC gas diffusion layers. *Electrochem Commun* 2007; 9: 2340–2345.

19. Jena A and Gupta K. Characterization of pore structure of fuel cell components containing hydrophobic and hydrophilic pores. In: *41st power sources conference*, 2005.

20. Landeryou M, Eames I and Cottenden A. Infiltration into inclined fibrous sheets. *J Fluid Mech* 2005; 529: 173–193.

21. Jaganathan S, Tafreshi HV and Pourdeyhimi B. A realistic modeling of fluid infiltration in thin fibrous sheets. *J Appl Phys* 2009; 105: 113522.

22. Ashari A and Tafreshi HV. General capillary pressure and relative permeability expressions for through–plane fluid transport in thin fibrous sheets. *Colloid Surf A* 2009; 346: 114.

23. Aslannejad H and Hassanizadeh SM. Study of hydraulic properties of uncoated paper: image analysis and pore-scale modeling. *Transp Porous Media* 2017; 120: 67–81.

24. Jaganathan S, Tafreshi HV, Shim E, et al. A study on compression-induced morphological changes of nonwoven fibrous materials. *Colloids Surf A* 2009; 337: 173–179.

25. Jena AK and Gupta KM. In-plane compression porometry of battery separators. *J Power Source* 1999; 80: 46–52.

26. Miller B and Tyomkin I. Liquid porosimetry: new methodology and applications. *J Col Int Sci* 1994; 62: 163–170.

27. Van Genuchten MTh. A closed-form equation for predicting the hydraulic conductivity of unsaturated soils. *Soil Sci Soc Am J* 1980; 44: 892–898.

28. Durner W. Hydraulic conductivity estimation for soils with heterogeneous pore structure. *Water Resour Res* 1994; 32: 211–223.

29. Brooks RH and Corey AT. *Hydraulic properties of porous media*. Hydrology Paper No. 3. Fort Collins, CO: Colorado State Univ., 1964.

30. Leverett MC. Capillary behavior in porous solids. *Trans Sot Pet Eng AlME* 1941; 142: 152–169.

31. Udell KS. Heat transfer in porous media considering phase change and capillarity-the heat pipe effect. *Int J Heat Mass Transf* 1985; 28: 485–495.

32. Pasaogullari U and Wang CY. Liquid water transport in gas diffusion layer of polymer electrolyte fuel cells. *J Electrochem. Soc* 2004; 151: A399–A406.

33. Pinder GF and Gray WG. *Essentials of multiphase flow in porous media*. Hoboken, NJ, USA: WileyInterscience, 2008.

34. Gerke HH and van Genuchten MTh. Evaluation of a first order water transfer term for variably saturated dual-porosity flow models. *Water Resour Res* 1993; 29: 1225–1238.

35. Hassanizadeh SM, Celia MA and Dahle HK. Dynamic effects in the capillary pressure-saturation relationship and their impacts on unsaturated flow. *Vadose Zone J* 2002; 1: 38–57.

36. Mohebbi B, Tavangarrad AH, Clausen J, et al. Revealing how interfaces in stacked thin fibrous layers affect liquid ingress and transport properties by single-sided NMR. *J Magn Resonan* 2018; 294: 16–23.